Air Pad Controlled by Means of a Diaphragm-Valve: Static and Dynamic Behaviour

Air Pad Controlled by means of a Diaphragm-Valve: Static and Dynamic Behaviour

Colombo F.[1[0000-0002-1054-236X]] Lentini L.[1[0000-0003-3770-3773]] Raparelli T.[1[0000-0003-0063-7733]] A Trivella[1[0000-0003-4664-7937]] Viktorov V.[1[0000-0002-7597-6142]]

[1] Politecnico di Torino, Corso Duca degli Abruzzi 24, Torino, 10129, Italy.
luigi.lentini@polito.it

Abstract. This paper presents the analysis of the static and dynamic performance of a passively compensated air pad. The proposed method consists in the integration of a custom-built diaphragm valve and a commercial aerostatic pad. A lumped model is used to simulate the static and dynamic performance of the pad. Results demonstrate that the proposed method is very effective when the system works with excitation frequencies below 10 Hz.

Keywords: compensation, aerostatic pad, diaphragm valve.

1 Introduction

Aerostatic bearings are used in applications where very high precision of positioning is required. In view of their almost zero friction, they are used in machine tools, measuring machines, semi-conductor manufacturing and power board testing [1].

However, air bearings suffer from low relative stiffness and poor damping. Many solutions have been proposed to increase aerostatic bearing stiffness and damping. Higher stiffness can be obtained by reducing the size of the supply holes and modifying their location. In this regard, Colombo et al. [2] and others [3, 4] investigated on the effect of the position and size of the supply holes of aerostatic pads. It was found that reducing the supply hole diameter makes it is possible to moderately increase the stiffness and simultaneously reduce the air consumption to the detriment of the load capacity.

Machining shallow grooves on the active surface of the pad, i.e., using compound restrictors, is another solution that makes it possible to increase stiffness and load capacity. Nakamura et al [5, 6] along with Colombo et al. [7] find that, given the air consumption, the use of compound restrictors can significantly increase the load capacity and the stiffness but reduces damping even compromising the stability of the pad. Moreover, recent advances in manufacturing allow the increase of stiffness using micro-holes [8]. The use of porous inserts, surfaces and metal woven wire cloth [9] makes it possible to obtain aerostatic bearing with higher load capacity, stiffness and damping. However, despite their higher performance, these solutions present some drawbacks related to their permeability, mechanical properties and integration.

More recently, different types of compensation methods have been proposed in order to obtain improvements in performance. These methods consist in integrating aerostatic pads with additional elements or devices in order to increase their performance. Raparelli et al. [10] presented a review on the subject providing a rigorous classification. Passive compensation methods use components which require only the energy associated with the supply pressure of the bearing, e.g., pneumatic valves and compliant elements. By contrast, active compensation methods exploit devices that require external sources of energy for their functioning. It was found that the more effective active compensation solutions are those exploiting the use of piezoelectric actuators used in a closed control loop where the feedback is provided by displacement sensors. This kind of active control can be used to modify the geometry or the pressure distribution of the pad. Al Bender [11] and Aguirre [12] proposed a protype of active circular pad where three piezo actuators were used to actively control the conicity of the air gap geometry. Similarly, Maamari et al. [13, 14] proposed an active aerostatic bearing based on conicity control by means of a magnetic actuation. Colombo et al.[15] proposed an alternative solution where a piezo actuator was integrated with a custom built compliant mechanism [16] to obtain a geometrical compensation.

Despite their higher effectiveness, active compensation solutions are still too expensive to be used in current industrial applications. Conversely, passive compensation solutions can be a cost-effective solution notwithstanding their lower dynamics. Most of the current passive compensation solutions exploit the presence of compliant elements, e.g., elastic orifice [17], compliant surfaces [18] or springs [19]. In spite of their ease of integration and relatively low cost, valves have rarely been integrated with aerostatic pads to obtain performance improvements [20].

This paper presents the study of the static and dynamic performance of a passively compensated pad that exploits a pneumatic diaphragm valve to enhance performance. The static performance of this system has been described in [21, 22], where the lumped model presented in [21] was suitably modified to investigate the static and dynamic behaviour of an optimally designed compensated system.

2 Materials and Methods

2.1 The compensated pad

The compensation method proposed consists in integrating a commercial pad with a custom-built diaphragm valve. Given the operating conditions of the pad and the designed features of the valve, it has been shown [21] that the bearing can exhibit a significant increase in stiffness up to a quasi-static infinite value. Figures 1a and 1b show the geometry of the valve and the commercial pad. The valve presents a chamber of volume V_1 which is supplied through a nozzle of diameter d_v. The presence of a diaphragm in the lower part of the valve makes it possible to change the volume of its chamber depending on the value of its interior pressure P_1. The diaphragm presents a thickness of s and a diameter d_m. The initial position between the nozzle and the diaphragm x_n can be manually regulated via a regulating screw whereas, the presence of a Belleville spring favours the regulation in the opposite direction and preloads the screw increasing the accuracy of the positioning. The structure of the valve is directly connected to the commercial pad through four screws. The pad presents a rectangular base of dimensions (AxB) 60x30 mm^2 and four orifices with a diameter (d_p) of 1 mm. Each restrictor is located in the middle of a grooved rectangular supply line with a base (a) of 45 mm and a depth (b) of 20 mm. The grooves present a triangular cross-section of base (w_g) 0.2 mm and a height (w_g) of 0.06 mm.

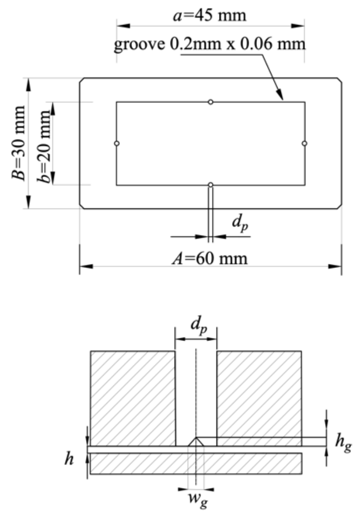

Fig. 1a: Pad geometry

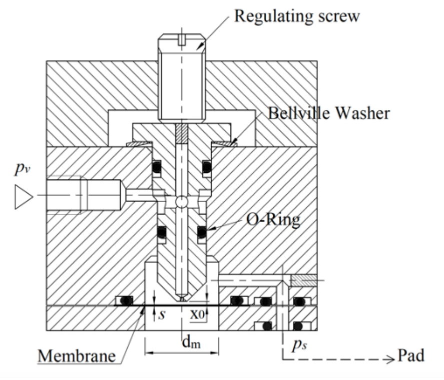

Fig. 1b: Valve geometry

2.2 The pad model

Starting from the upstream, the nozzle supplies a mass flow rate G_1 which depends on its distance x from the diaphragm. As can be seen, this distance is the sum of the initial diaphragm-nozzle distance x_n and the diaphragm deflection x_v (see Equation 1b). In some operating conditions the nozzle can be used to impose an initial preload to the diaphragm (x_n) and this distance is measured in the opposite direction with respect to x_v.

Figure 2 shows the functional scheme of the compensated pad. The system is modelled as a pneumatic circuit composed of lumped resistances and volumes. It was experimentally found that the valve works as a constant pneumatic resistance when $x \leq 12\ \mu m$ and regulates when $x > 12\mu m$. To take into account this phenomenon, the diaphragm deflection was computed as follows:

$$\begin{cases} x = 12\ \mu m; & x \leq 12\ \mu m \quad (1a) \\ x = x_n + \overbrace{\frac{\pi {d_m}^2}{4} \frac{(P_1 - P_a)}{k_m}}^{x_v}; & x > 12\mu m \quad (1b) \end{cases}$$

where, k_m is the equivalent mono-dimensional stiffness of the diaphragm and P_1 and P_a are the valve and ambient absolute pressures. The air mass flow rate G_1 is computed by means of the following formula [23]:

$$G_1 = K_T \overbrace{1.05(1-0.3\,e^{-0.005\,Re_v})}^{cd_v} \frac{0.685}{\sqrt{R\,T}}\,\pi\,d_v\,x\,P_s \sqrt{1-\left(\frac{\frac{P_1}{Ps}-b_c}{1-b_c}\right)^2} \qquad (2)$$

where, K_T is square root of the ratio between a reference absolute temperature (273 K) and the temperature in the valve (293 K). The discharge coefficient of the nozzle cd_v is computed according to [24], $Re_v = {G_1}/{\pi \mu d_v}$ is the related Reynolds number related and b_c is the theoretical critical pressure ratio (0.528).

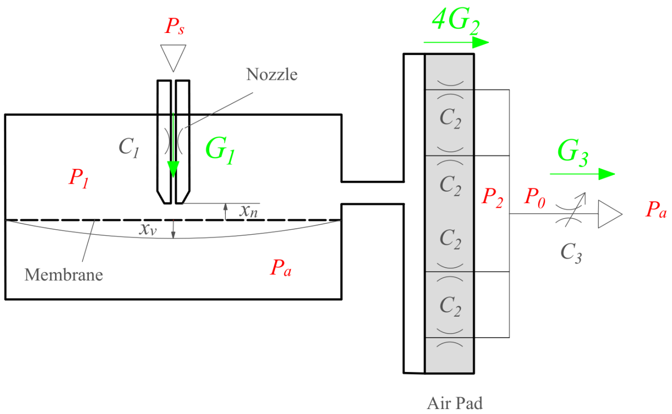

Fig. 2: Functional scheme of the compensated pad.

Similarly, the mass flow rate passing through the supply holes of the pad is computed as:

$$G_2 = K_T 1.05(1-0.3\,e^{-0.005\,Re_a}) \frac{0.685}{\sqrt{R\,T}}\,A_{eqv} P_1 \sqrt{1-\left(\frac{\frac{P_2}{P_1}-b_c}{1-b_c}\right)^2} \qquad (3)$$

where, to take into account the presence of the grooves an equivalent area A_{eqv} and a modified Reynolds number Re_a were introduced.

$$A_{eqv} = \pi\,d_p\,h + 2\,w_g\,h_g \qquad (4)$$

$$Re_a = \frac{G_2\, h}{\mu\left(\pi d_p h + 2w_g\ h_g\right)} \tag{5}$$

These two mass flow rates are used in the continuity equation applied at the volume of the valve V_1 to compute the related pressure P_1:

$$G_1 - 4G_2 = \frac{V_1}{RT}\frac{dP_1}{dt} + \frac{P_1}{RT}\frac{\pi {d_m}^2}{4}\frac{dx}{dt} \tag{6}$$

Similarly, the continuity equation applied at the air gap volume V_0 is used to compute the pressure downstream the supply holes P_2:

$$4G_2 - G_3 = \frac{P_2 A_0}{RT}\frac{dh}{dt} + \frac{(Ah + V_g)}{RT}\frac{dP_2}{dt} \tag{7}$$

where V_g is the grooves volume and G_3 is the laminar mass flow rate exhausted from the air gap:

$$G_3 = \frac{1}{6\mu RT}\left(\frac{b}{A-a} + \frac{a}{B-b}\right)(P_0^2 - P_a^2)h^3 \tag{8}$$

The air gap pressure distribution within central volume under the rectangular area bordered by the grooves is considered constant and related to the pressure P_2 through the following semi-empirical formula:

$$P_0 = \left[1 - 0.14^{\left(\frac{5}{h}\right)}\right](P_2 - P_a) + P_a \tag{9}$$

where, h is expressed in μm.

The load capacity of the pad is computed by assuming a linear pressure distribution outside the area surrounded by the grooves:

$$F_p = \left[ab + AB + \frac{(Ab + aB)}{2}\right]\frac{(P_0 - P_a)}{3} \tag{10}$$

Since the compensating action of the valve introduces a form of non-linearity renders the load capacity F_p a non-injective function of the air gap height h[1], conventional procedures cannot be employed. In view of this, the values of air gap heights are computed through the equilibrium equation of the pad by imposing the external load applied to the pad F^{ext}:

$$F_p = F^{ext} + M\ddot{h} \tag{11}$$

[1] There can be more than one possible load capacity for the same air gap height.

where, M is the mass supported by the pad. The lumped model is implemented using Euler explicit method assuming a time step of 10^{-7} s. The static curves of the system are obtained starting from an initial equilibrium condition[2] (h_0, F_{p_0}, G_0, P_{0_0}, P_{1_0}, P_{2_0}) and selecting the resolution of the load capacity curve ΔF. The external load F^{ext} acting on the pad is thus computed as:

$$F_i^{ext} = F_{p_0} + i \cdot \Delta F \tag{12}$$

where, i corresponds to the i^{th} static operating condition of the pad ($i = 0, 1, 2, \dots, i_{max}$). In each step ($i$), the equilibrium air gap height is computed by iteratively solving equations (6), (7) and (10) till the equilibrium of the pad is reached $M\ddot{h} \cong 0$. The dynamic features of the pad (dynamic stiffness k_{dyn} and damping c) are compute by imposing sinusoidal variation of the external force $\Delta F_i^{ext} = 0.05 F_i^{ext} \cdot \sin(2\pi f_k)$ for each equilibrium point of the curve and computing the FFT of the ratio between the air gap force $F_p(t)$ and displacement $h(t)$.

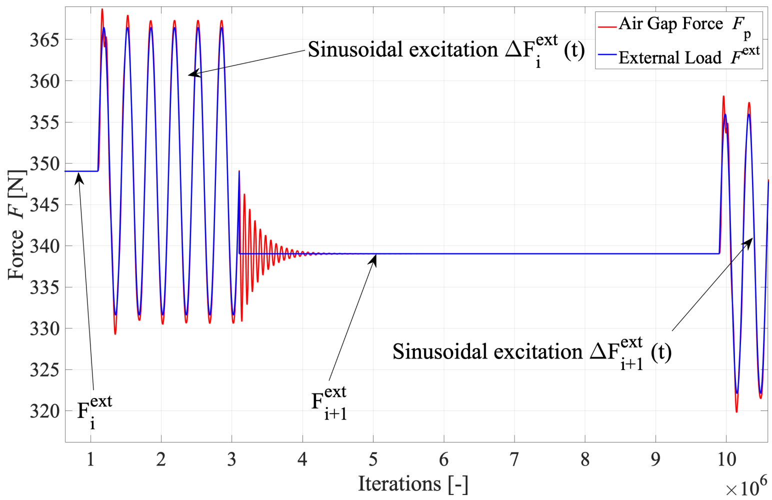

Fig. 3: Dynamic trend of the external force F^{ext} and the air gap force F_p.

Figure 3 shows the dynamic trend of the external force F^{ext} and the air gap force F_p during two consecutive equilibrium conditions.

[2] This condition is obtained solving the iterative set of equations (6), (7), (11) for F_p. This corresponds to point D in Figures 4, 5 and 6.

3 Results and Discussions

The accuracy of the proposed static model was demonstrated in [21]. The present research investigates the results of an optimized version of the compensated system. The optimal parameters of the valve are computed: k_m=2.6 10^5 N/m, x_n=-7.5 μm, d_v=0.38 mm and d_m=5.5 mm, after selecting the type of passive pad (see section 2.1) and its operating conditions (absolute supply pressure P_s=0.525 MPa and air gap height h^*=8.25 μm). These optimal values make it possible to obtain the maximum stiffness avoiding the presence of negative stiffness (further details are given in [21]).

3.1 Static performance

Figures 4-6 show the static curves of the optimized compensated pad. In these figures it is possible to distinguish a by-pass ($\overline{AB}$), regulation ($\overline{BC}$) and a saturation ($\overline{CD}$) zones.

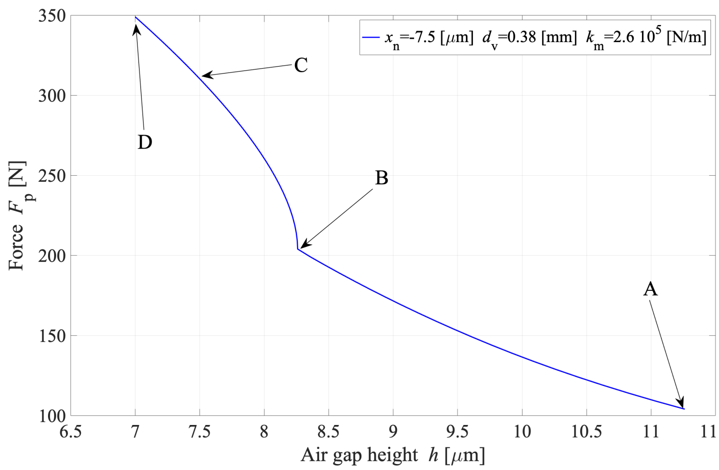

Fig. 4: Load Capacity of the compensated pad.

In the by-pass region $\overline{AB}$ the valve works as a constant pneumatic resistance because of the initial preload applied to the diaphragm (x_n=-7.5 μm). This is because the load applied to the pad is not sufficient to create a sufficient pressure P_1 nor a well-defined clearance between the nozzle and the diaphragms. In fact, experimental results demonstrate that the mass flow rate supplied to the pad is provided due to the incomplete closure of the valve nozzle. The by-pass region ends when the pressure P_1 is sufficiently high to create a well-defined clearance between the nozzle and the diaphragm (B). When this occurs, the valve starts regulating. The valve action makes it possible to compensate the air gap variations induced due to external load variations by increasing the mass flow rate provided to the pad. In fact, as can be seen, the air consumption of the pad sharply increases making it possible to obtain an extremely strong rise of the stiffness ($\overline{BC}$).

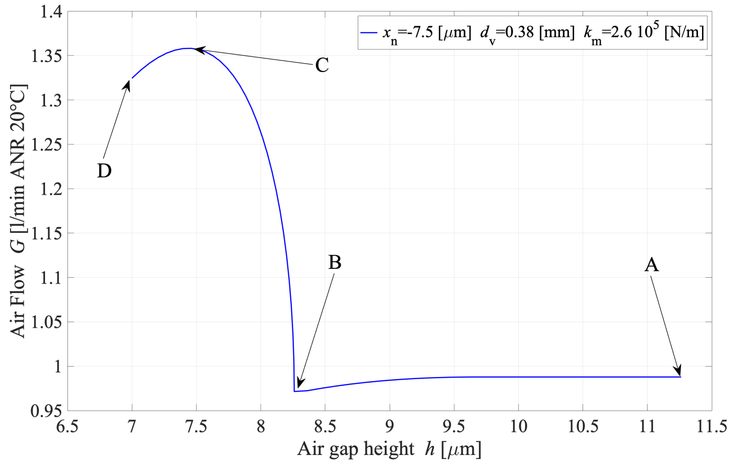

Fig. 5: Air consumption of the compensated pad.

The valve regulation ends when the increase of the distance between the nozzle and the diaphragm generates the nozzle saturation. This point (C) corresponds to the maximum air consumption and stiffness of the pad. From this condition, further increases of the applied load can no longer be compensated by the valve. This produces a simultaneous reduction of stiffness and air consumption.

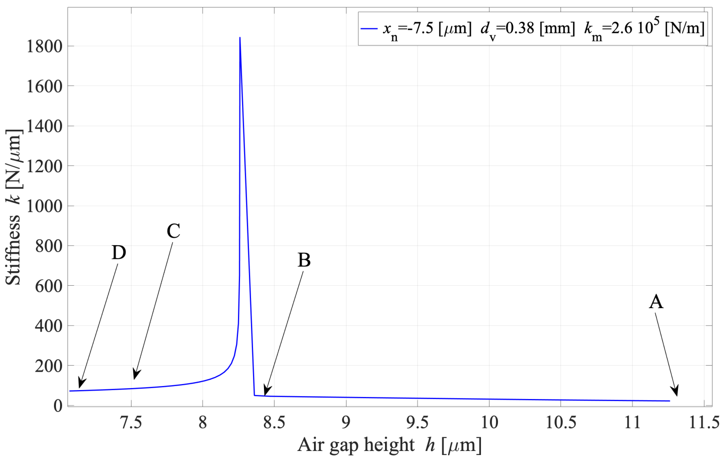

Fig. 6: Stiffness of the compensated pad.

3.2 Dynamic Performance

The quasi-static stability of the system was already proven through step force tests in a previous work [21]. The aim of this paper is to assess the stability of the system at various excitation frequencies. The dynamic performance of the pad is numerically evaluated in a frequency range from 1 to 100 Hz through the application of sinusoidal loads $\Delta F_i^{ext} = 0.05 F_i^{ext} \cdot \sin(2\pi f_k)$. The BIBO[3] stability is evaluated by considering the sign of the air pad damping over the frequency range of interest. This is because it is has been established that air pads are stable till they exhibit positive damping [11, 14]. Dynamic stiffness and damping are computed point by point from the magnitude $|1/H(j\omega)|$ and the phase $\arg(1/H)$ of the inverse of $\mathrm{FFT}\left[h(t)/F_p(t)\right]$:

$$H(j\omega) = \frac{F_p(j\omega)}{h(j\omega)} = \overbrace{k_{dyn}(j\omega)}^{Re(H)} + j\,\overbrace{2\pi f c(j\omega)}^{Im(H)} \tag{12}$$

where, $Re(H)$ and $Im(H)$ are the real and imaginary part of the transfer function $H(j\omega)$. Figure 7 shows the trend of the dynamic stiffness k_{dyn} of the pad expressed as a function of the excitation frequency f. As can be seen, the stiffness presents a dramatic reduction moving from 1 to 5 Hz and remains almost constant above this frequency. Moreover, in contrast with static stiffness, dynamic stiffness decreases monotonically as the applied static preload is reduced.

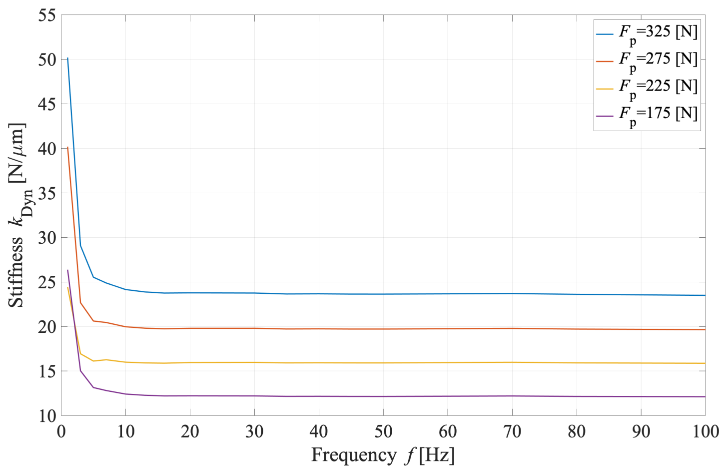

Fig. 7: Dynamic stiffness k_{dyn} vs frequency f.

The air pad damping exhibits a similar trend moving from 1 to 5 Hz but, above this frequency, it continues to slightly decrease, becoming negative at about 55 Hz (see Figure 8). It is also worth noting that in the lower frequency range (from 1 to 5 Hz) the

[3] Bounded Input Bounded Output.

pad presents values of damping that are very high compared to those of conventional pads.

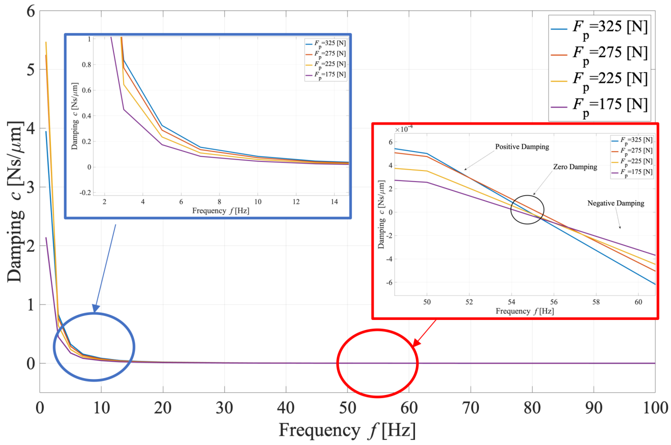

Fig. 8: Damping c vs frequency f

The dramatic reduction of the pad stiffness and damping can be explained by the low dynamics of the pneumatic valve. In fact, as the frequency increases, the compensating action of the valve gradually loses its effectiveness. Figure 9 shows the trends of the variations of the valve (Inflow G_1) and the air gap (Outflow G_3) flow rate at 10 Hz. It can be seen that the oscillations of the valve mass flow rate exhibit a lower amplitude compared to that of the air gap. Further investigations at higher frequency demonstrate that this phenomenon becomes more prominent as the frequency increases.

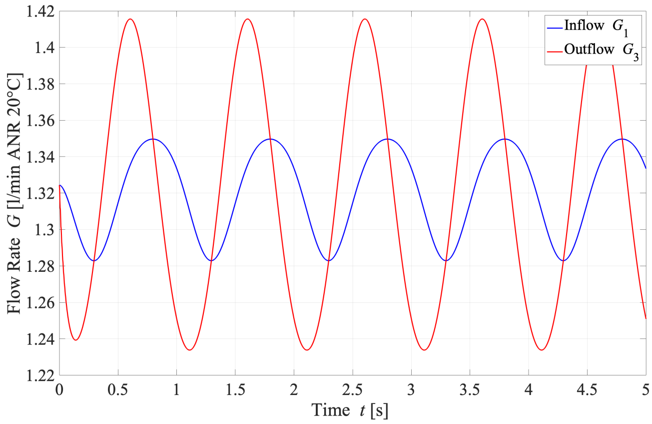

Fig. 9: Dynamic trend of the valve G_1 and the air gap G_3 flow rates.

4 Conclusions

This paper presented a numerical investigation on the static and dynamic performance of a passively compensated aerostatic pad. The passive compensation method consists in the integration of a custom-built diaphragm valve and a commercial pad. The main parameters of the valve were selected to obtain an optimal design for the considered operating conditions of the system. Once the valve parameters was designed, the static and dynamic performance was evaluated. Static results demonstrated that this compensation method makes it possible to significantly increase the stiffness of the pad around the selected operating condition of the pad. The dynamic analysis revealed that the performance of the proposed compensation method dramatically decreases as the frequency increases due to the low dynamics of the valve. These results indicate that this compensation method represents an efficient and cost-effective method for the typical (low frequency) air pad applications.

References

1. Lentini, L., Moradi, M., Colombo, F.: A Historical Review of Gas Lubrication: From Reynolds to Active Compensations. Tribology in Industry. 40, 165–182 (2018). https://doi.org/10.24874/ti.2018.40.02.01
2. Colombo, F., Lentini, L., Raparelli, T., Trivella, A., Viktorov, V.: Dynamic Characterisation of Rectangular Aerostatic Pads with Multiple Inherent Orifices. Tribology Letters. 66, (2018). https://doi.org/10.1007/s11249-018-1087-x
3. Kassab, S.Z., Noureldeen, E.M., Shawky, M.A.: Effects of operating conditions and supply hole diameter on the performance of a rectangular aerostatic bearing. Tribology international. 30, 533–545 (1997)
4. Boffey, D.A., Duncan, A.E., Dearden, J.K.: An experimental investigation of the effect of orifice restrictor size on the stiffness of an industrial air lubricated thrust bearing. Tribology International. 14, 287–291 (1981)
5. Nakamura, T., Yoshimoto, S.: Static tilt characteristics of aerostatic rectangular double-pad thrust bearings with compound restrictors. Tribology international. 29, 145–152 (1996)
6. Yoshimoto, S., Tamura, J., Nakamura, T.: Dynamic tilt characteristics of aerostatic rectangular double-pad thrust bearings with compound restrictors. Tribology International. 32, 731–738 (1999). https://doi.org/10.1016/S0301-679X(00)00004-9
7. Colombo, F., Lentini, L., Raparelli, T., Trivella, A., Viktorov, V.: Dynamic model of a grooved thrust bearing: Numerical model and experimental validation. Presented at the (2017)
8. Belforte, G., Colombo, F., Raparelli, T., Trivella, A., Viktorov, V.: Experimental Analysis of Air Pads with Micro Holes. Tribology Transactions. 56, 169–177 (2013). https://doi.org/10.1080/10402004.2012.734547
9. Belforte, G., Raparelli, T., Viktorov, V., Trivella, A.: Metal woven wire cloth feeding system for gas bearings. Tribology International. 42, 600–608 (2009). https://doi.org/10.1016/j.triboint.2008.06.001

10. Raparelli, T., Viktorov, V., Colombo, F., Lentini, L.: Aerostatic thrust bearings active compensation: Critical review. Precision Engineering. 44, 1–12 (2016). http://dx.doi.org/10.1016/j.precisioneng.2015.11.002

11. Al-Bender, F.: On the modelling of the dynamic characteristics of aerostatic bearing films: From stability analysis to active compensation. Precision Engineering. 33, 117–126 (2009). http://dx.doi.org/10.1016/j.precisioneng.2008.06.003

12. Aguirre, G., Al-Bender, F., Van Brussel, H.: A multiphysics model for optimizing the design of active aerostatic thrust bearings. Precision Engineering. 34, 507–515 (2010). https://doi.org/10.1016/j.precisioneng.2010.01.004

13. Maamari, N., Krebs, A., Weikert, S., Wegener, K.: Centrally fed orifice based active aerostatic bearing with quasi-infinite static stiffness and high servo compliance. Tribology International. 129, 297–313 (2019)

14. Maamari, N., Krebs, A., Weikert, S., Wild, H., Wegener, K.: Stability and dynamics of an orifice based aerostatic bearing with a compliant back plate. Tribology International. 138, 279–296 (2019)

15. Colombo, F., Lentini, L., Raparelli, T., Viktorov, V.: Actively compensated aerostatic thrust bearing: design, modelling and experimental validation. Meccanica. 1–16 (2017). https://doi.org/10.1007/s11012-017-0689-y

16. Colombo, F., Lentini, L., Raparelli, T., Viktorov, V.: A Compliant mechanism for Aerostatic Thrust Bearings Controlled by Piezo-actuators. International Journal of Applied Engineering Research. 12, 7803–7815 (2017)

17. Newgard, P.M., Kiang, R.L.: Elastic Orifices for Pressurized Gas Bearings. A S L E Transactions. 9, 311–317 (1966). https://doi.org/10.1080/05698196608972147

18. Holster, P.L., Jacobs, J.A.H.: Theoretical analysis and experimental verification on the static properties of externally pressurized air-bearing pads with load compensation. Tribology International. 20, 276–289 (1987). http://dx.doi.org/10.1016/0301-679X(87)90028-4

19. Chen, M.-F., Lin, Y.-T.: Dynamic Analysis of the X-shaped Groove Aerostatic Bearings with Disk-Spring Compensator. JSME International Journal Series C. 45, 492–501 (2002). https://doi.org/10.1299/jsmec.45.492

20. Colombo, F., Maffiodo, D., Raparelli, T.: Active Gas Thrust Bearing With Embedded Digital Valves and Backpressure Sensors. Tribology Transactions. 60, 807–813 (2017). https://doi.org/10.1080/10402004.2016.1213344

21. Ghodsiyeh, D., Colombo, F., Lentini, L., Raparelli, T., Trivella, A., Viktorov, V.: An infinite stiffness aerostatic pad with a diaphragm valve. Tribology International. 141, 105964 (2020)

22. Ghodsiyeh, D., Colombo, F., Raparelli, T., Trivella, A., Viktorov, V.: Diaphragm valve-controlled air thrust bearing. (2016)

23. Belforte, G., Raparelli, T., Viktorov, V.: Modeling and identification of gas journal bearings: self-acting gas bearing results. Journal of tribology. 124, 716–724 (2002)

24. Colombo, F., Lentini, L., Raparelli, T., Trivella, A., Viktorov, V.: A Lumped Model for Grooved Aerostatic Pad. In: Advances in Service and Industrial Robotics. pp. 678–686. Springer International Publishing (2019)